ISSN 1063-7710, Acoustical Physics, 2016, Vol. 62, No. 4, pp. 418–428. © Pleiades Publishing, Ltd., 2016.
Original Russian Text © O.V. Rudenko, S.N. Gurbatov, 2016, published in Akusticheskii Zhurnal, 2016, Vol. 62, No. 4, pp. 412–423.

NONLINEAR ACOUSTCIS

Inverse Problem of Nonlinear Acoustics: Synthesizing Intense Signals to Intensify the Thermal and Radiation Action of Ultrasound

O. V. Rudenko[a, b, c, d, e] and S. N. Gurbatov[b]

[a] *Moscow State University, Physics Faculty, Moscow, 119991 Russia*
[b] *Nizhny Novgorod State University, pr. Gagarina 23, Nizhny Novgorod, 603950 Russia*
[c] *Prokhorov General Physics Institute, Russian Academy of Sciences, ul. Vavilova 38, Moscow, 119991 Russia*
[d] *Schmidt Institute of Physics of the Earth, Russian Academy of Sciences, ul. Bol'shaya Gruzinskaya 10/1, Moscow, 123242 Russia*
[e] *School of Engineering, Blekinge Institute of Technology, 371 79 Karlskrona, Sweden*
e-mail: rudenko@acs366.phys.msu.ru

Received November 6, 2015

Abstract—Inverse problems of nonlinear acoustics have important applied significance. On the one hand, they are necessary for nonlinear diagnostics of media, materials, manufactured articles, building units, and biological and geological structures. On the other hand, they are needed for creating devices that ensure optimal action of acoustic radiation on a target. However, despite the many promising applications, this direction remains underdeveloped, especially for strongly distorted high-intensity waves containing shock fronts. An example of such an inverse problem is synthesis of the spatiotemporal structure of a field in a radiating system that ensures the highest possible energy density in the focal region. This problem is also related to the urgent problems of localizing wave energy and the theory of strongly nonlinear waves. Below we analyze some quite general and simple inverse nonlinear problems.

Keywords: nonlinearity, diagnostics, inverse problem, shock wave, focusing
DOI: 10.1134/S1063771016040163

INTRODUCTION

The term "inverse problem of nonlinear acoustics" (IPNA) was used by one of the authors in review [1], devoted to the 70th birthday of R.V. Khoklov. Later, this review was published in [2]. In these years, tomographic problems began do be solved [3], which were directed at reconstructing the spatial distribution of the nonlinear elasticity moduli of a medium from acoustic scattering data. Today, such nonlinear problems are being actively studied in relation to creating medical tomographs [4]. The number of inverse problems also includes estimation of the contact roughness of abutting surfaces [5], methods for profiling channels of variable cross section [6], and nonlinear diagnostics of media [7]. The stages of formulating the corresponding direction—nonlinear acoustic diagnostics—are reflected in reviews [8, 9]. Nonlinear diagnostics have acquired a special role in medical applications [10].

However, despite the important applied orientation, the basic aspects of this direction remain underdeveloped. A particular lag behind current requirements is observed in studying IPNA related to strongly distorted high-intensity waves containing shock fronts. An example is synthesis of the spatiotemporal structure of a field in a radiating system that ensures high-density energy of the field in the focal region. This is related to the important physical problems of localizing wave energy and to the theory of strongly nonlinear waves [11]. Below we discuss formulation and analysis of IPNA.

INTENSIFICATION OF ACTION DURING SHOCK FRONT FORMATION

We show using simple examples how to intensify the action on a medium via shock front formation. We will proceed from a Burgers-type equation or its generalization to wave beams—the KZK equation [12–16].

In order to simplify writing of the formulas that will appear as a result of calculations, we write the general equation for an axially symmetric beam in normalized form:

$$\frac{\partial}{\partial\theta}\left(\frac{\partial V}{\partial z}-V\frac{\partial V}{\partial\theta}-\Gamma\frac{\partial^2 V}{\partial\theta^2}\right)=\frac{N}{4}\left(\frac{\partial^2 V}{\partial R^2}+\frac{1}{R}\frac{\partial V}{\partial R}\right). \quad (1)$$

When writing (1), dimensionless variables are used:

$$V=\frac{p}{p_0},\quad z=\frac{x}{l_{SH}},\quad \theta=\omega\tau,\quad R=\frac{r}{a}. \quad (2)$$

Here, p is acoustic pressure and x is a coordinate along the beam axis. The axis coincides with the direction of wave propagation. Further, r is a coordinate in the plane orthogonal to the beam axis, and $\tau = t - x/c_0$ is

time in a coordinate system moving along with the wave at sound velocity c_0. Variables (2) are normalized to the amplitude value of pressure p_0, characteristic wave frequency ω, characteristic beam radius a, and nonlinear length l_{SH}, the distance at which a discontinuity forms in a plane wave harmonic at the input. In addition to scale l_{SH}, Eq. (1) has two other parameters with the dimension of length. These are the characteristic distances of the manifestation of diffraction and dissipative effects:

$$l_{SH} = \frac{c_0^3\rho_0}{\varepsilon\omega p_0}, \quad l_{DIF} = \frac{\omega a^2}{2c_0}, \quad l_{DISS} = \frac{2c_0^3\rho_0}{b\omega^2}. \tag{3}$$

The ratios of these lengths form two dimensionless numbers:

$$\Gamma = \frac{l_{SH}}{l_{DISS}}, \quad N = \frac{l_{SH}}{l_{DIF}}. \tag{4}$$

The case of strongly pronounced nonlinearity corresponds to the smallness of numbers (4). Here, the nonlinear effects manifest themselves at smaller distances than dissipative and diffraction phenomena.

Let us first consider plane waves. Ignoring the dependence of acoustic field on transverse coordinate R, we obtain the Burgers equation from Eq. (1) [13, 14]. Hence follows the integral relation

$$\frac{\partial\overline{V^2}}{\partial z} - \frac{2}{3}\frac{\overline{\partial V^3}}{\partial\theta} = 2\Gamma\overline{V\frac{\partial^2 V}{\partial\theta^2}}. \tag{5}$$

Here, the overbar means averaging over the period (if the signal is periodic in time) or integration over the entire domain of variable θ in which the signal at a given point in space differs from zero. Since the mean from the derivative $\partial/\partial\theta$ is equal to zero, relation (5) transforms to

$$\frac{\partial\overline{V^2}}{\partial z} = -2\Gamma\overline{\left(\frac{\partial V}{\partial\theta}\right)^2} = -Q. \tag{6}$$

The left-hand side of (6) is proportional to the decay rate of the volumetric density of energy E transferred by the wave, or of its intensity I:

$$\overline{V^2} = \frac{c_0^2\rho_0}{p_0}E, \quad E = \frac{I}{c_0} = \frac{\overline{p^2}}{c_0^2\rho_0}. \tag{7}$$

For the harmonic initial wave propagating in a dissipative medium according to the laws of linear acoustics, from (6) follows the obvious result: amplitude $A(z)$ attenuates by an exponential law:

$$V = A(z)\sin\omega\theta,$$
$$\frac{dA^2}{dz} = -2\Gamma A^2, \quad A^2 = \exp(-2\Gamma z). \tag{8}$$

For a single shock wave with a normalized pressure jump $A(z)$, we obtain from formula (6) [13]

$$V = A(z)\,\mathrm{th}\left[\frac{\theta}{2\Gamma}A(z)\right], \quad \frac{\partial\overline{V^2}}{\partial z} = -\frac{4}{3}A^3(z). \tag{9}$$

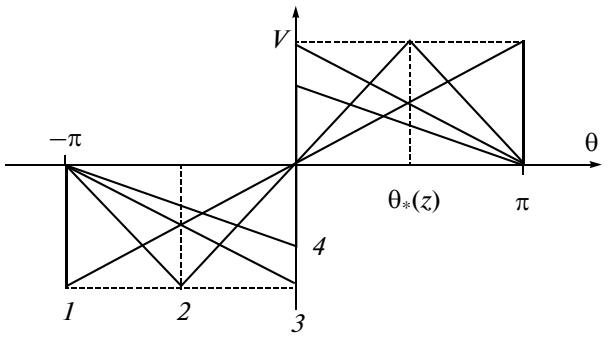

Fig. 1. Nonlinear evolution of "inverse saw" (curve *1*)—its transformation into a common saw-tooth wave (curve *3*) attenuating due to shock front formation. The increase in the number of curves *1–4* corresponds to an increase in distance passed by the wave in a nonlinear medium.

In contrast to linear attenuation (8), which depends on the dissipative properties of the medium (or on number Γ), nonlinear attenuation is determined only by the pressure jump $A(z)$ at the shock front; it does not depend on number Γ. In addition, in contrast to a periodic signal having a finite energy $\overline{V^2} = A^2/2$, for shock wave (9), integral $\overline{V^2}$ should be calculated in infinite limits. Here, the integral diverges, whereas the energy decay rate with distance $Q = -d\overline{V^2}/dz$ is finite. Thus, when using relation (6) in different cases, it is convenient to calculate either its left- or right-hand side.

In cases when the dissipation is weak ($\Gamma \ll 1$), and there is no discontinuity, it is possible to approximately calculate losses after substituting into the right-hand side of (6) the solution for a nonlinear Riemann (simple) wave:

$$V = \Phi(\theta + zV). \tag{10}$$

Here, $\Phi(\theta)$ is an arbitrary function giving the initial waveform for $z = 0$. The result for periodic ($-\pi < \theta < \pi$) and aperiodic ($-\infty < \theta < \infty$) signals has the form

$$Q = \frac{\Gamma}{\pi}\int_{-\pi}^{\pi}\frac{\Phi'^2(\xi)}{1 - z\Phi'(\xi)}d\xi, \quad Q = 2\Gamma\int_{-\infty}^{\infty}\frac{\Phi'^2(\xi)}{1 - z\Phi'(\xi)}d\xi. \tag{11}$$

As an example, let us consider a periodic signal in the form of an "inverse saw." One of its periods is shown by curve *1* in Fig. 1. During propagation, the profile sequentially takes the shape shown by curves *2–4*. After a steep leading edge forms (curve *3*), nonlinear attenuation begins—a decrease in the peak pressure (curve *4*) and wave energy independent of the dissipative parameters of the medium.

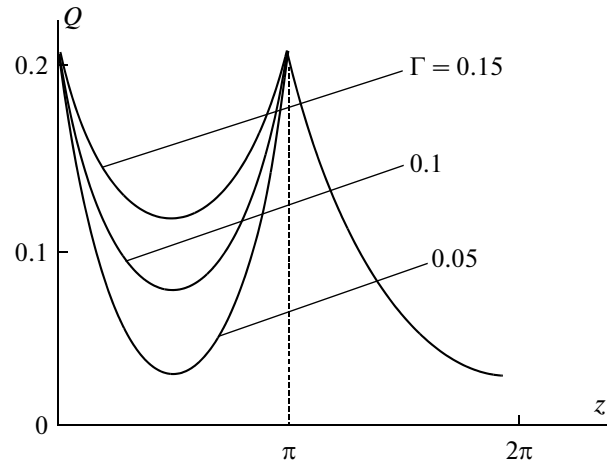

Fig. 2. Distance dependence of energy loss rate inverse saw (13), (14). The peak for $z = \pi$ is related to onset of nonlinear losses.

The wave profile is described by the Riemann solution, which for the positive half-period of the wave in Fig. 1 has the form

$$V(z,\theta) = \frac{\theta}{\pi - z}, \quad 0 < \theta < \theta_*(z) = \pi - z;$$
$$V(z,\theta) = \frac{\pi - \theta}{z}, \quad \theta_*(z) < \theta < \pi. \tag{12}$$

Calculation of losses using formula (11) yields

$$Q = \frac{2\Gamma}{z(\pi - z)}. \tag{13}$$

Clearly, the loss rate has two peculiarities: for $z = 0$ and $z = \pi$, which result from the infinitely large values of derivative $\partial V/\partial\theta$. In the vicinity of these peculiarities, it is necessary to take into account that the steepness of the front in a medium with finite attenuation, which is determined by its duration $\theta_{FR} = 2\Gamma/A(z)$, $A(\pi) = 1$, cannot exceed θ_{FR}^{-1}. From (11), we find that the finite value for Q, which can be estimated as $Q \approx \Gamma(\partial V/\partial\theta)^2\theta_{FR}$, does not depend on viscosity coefficient Γ. If we consider that for $z \approx \pi$, the shape of the shock front of the wave coincides with the shape of stationary shock front (9), then we obtain $Q = 2/(3\pi)$.

At distances $z > \pi$, a saw-tooth wave forms, which attenuations due to nonlinearity. For it,

$$V(z,\theta) = \frac{\pi - \theta}{z}, \quad 0 < \theta < \pi; \quad Q = \frac{2}{3}\frac{\pi^2}{z^3}. \tag{14}$$

The latter result is obtained from formula (9) under the assumption that for small attenuation coefficients, the wave front of the attenuating wave coincides with the stationary wave front. Since for $z = \pi$, the amplitude of the jump $A(\pi) = 1$ and averaging over the period is performed, i.e., result (9) needs to be divided by 2π, we obtain $Q = 2/(3\pi)$.

This is exactly the formula that is obtained from expression (14) if we set in it $z = \pi$. Since the curvature of the front, which is determined by its duration $\theta_{FR} = 2\Gamma/A(z)$, cannot exceed values of θ_{FR}^{-1}, the singularities for $z = 0$ and $z = \pi$ should be replaced by the finite value $Q = 2/(3\pi)$ obtained above.

Dependence (13), (14) of the loss rate on distance is shown in Fig. 2 for different values $\Gamma = 0.05$, 0.1, 0.15. The ratio of the maximum rate of nonlinear losses (achievable for $z = \pi$) to the minimum rate of linear losses is

$$K_* = \frac{Q_{NEL}}{Q_{LIN}} = \frac{\pi}{12\Gamma}. \tag{16}$$

For a value of the inverse acoustic Reynolds number $\Gamma = 10^{-2}$, we obtain $K_* \approx 25$, i.e., nonlinear losses are substantially stronger than linear losses, and the peak in Fig. 2 for $z = \pi$ is well pronounced.

Let us now consider a wave harmonic at the input $z = 0$, and set in the first formula (11) $\Phi = \sin\xi$. For the loss rate in the domain up to the formation of a discontinuity $z < 1$ we obtain

$$Q = 2\Gamma\frac{1 - \sqrt{1 - z^2}}{z^2\sqrt{1 - z^2}}. \tag{17}$$

At small distances $Q \approx \Gamma$, as also follows from linear theory (8). With an increase in z, higher harmonics are generated, which are absorbed more strongly, and quantity Q increases.

For $z = 1$, at the leading edge of the wave, a discontinuity forms, and formula (17) becomes useless. At distances $z \geq 1$, it is possible to use solution (9), but it must be taken into account that the Riemann wave profile is "cut" by the shock front. In the case of $\Phi = \sin\xi$, the front occupies the position $\theta = 0$ in the coordinate system accompanying the wave. Therefore, the "amplitude" $A(z)$ of the discontinuity is found from Eq. (9):

$$A = \sin(zA). \tag{18}$$

It is easy to see that $A(z = 1) = 0$. With an increase in distance z from 1 to $\pi/2$ amplitude $A(z)$ increases from zero to the maximum value $A(\pi/2) = 1$. Then, it asymptotically tends to zero for $z \to \infty$. At distances somewhat exceeding unity, and at large distances $z > 3$ approximate formulas [14] are valid:

$$A \approx \sqrt{6(z-1)}, \quad A \approx \frac{\pi}{1+z}. \tag{19}$$

Taking this into account, we calculate the mean wave energy:

$$\overline{V^2} = \frac{1}{\pi}\int_{\xi_*}^{\pi}\sin^2\xi(1 - z\cos\xi)d\xi. \tag{20}$$

The position of the front $\xi_*(z)$ is determined from the equation

$$\theta = \xi_*(z) - z\sin\xi_*(z) = 0, \quad \xi_*(z) = zA(z). \qquad (21)$$

Taking into account (21), we calculate energy (20):

$$\overline{V^2} = \frac{1}{2\pi}\left(\pi - zA + A\sqrt{1-A^2} + \frac{2}{3}zA^3\right). \qquad (22)$$

Differentiating (22) over z and taking into account the expression for the derivative of the amplitude,

$$\frac{dA}{dz} = \frac{A\sqrt{1-A^2}}{1 - z\sqrt{1-A^2}}, \qquad (23)$$

which is obtained from formula (18), we find

$$Q = -\frac{\partial\overline{V^2}}{\partial z} = \frac{2}{3\pi}A^3(z). \qquad (24)$$

Result (24) differs from (9) and (14) only by the fact that here, as the function $A(z)$, it is necessary to use the specific solution to Eq. (18). Figure 3 shows the distance dependence of the attenuation rate of the wave energy density, the initial shape of which is harmonic.

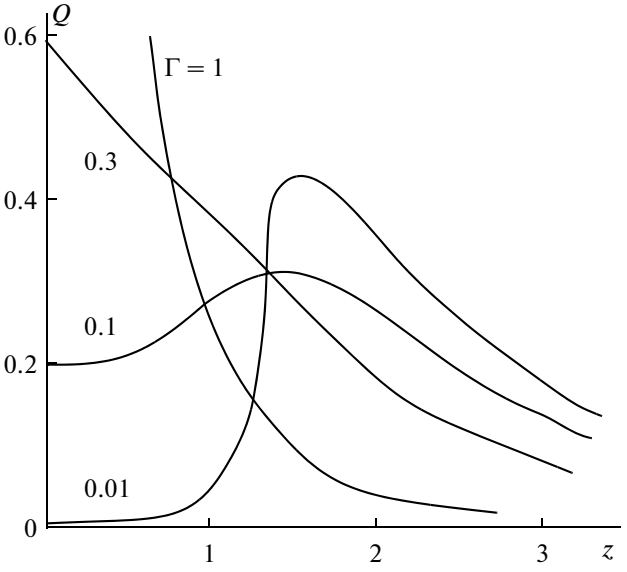

Fig. 3. Distance dependence of energy loss rate for wave harmonic at $z = 0$. The peak at $z = \pi/2$ corresponds to the maximum value of the formed shock front.

INVERSE PROBLEM OF NONLINEAR TIME FOCUSING

In dispersive media, when the wave propagation velocity depends on frequency, the decrease in the pulse duration (compression) due to a controlled change in the phase relations between harmonics is usually called time focusing [13].

In nonlinear acoustics, it makes sense to use this term as applied to a somewhat different phenomenon. It is well known that for vanishingly small viscosity, the solution to the Burgers equation can be interpreted as a flow of noninteracting particles with perfectly inelastic collisions [15, 16]. As well, the formation of a discontinuity corresponds to adhesion of particles and the formation of a heavy macroparticle, the position and velocity of which coincide with the discontinuity velocity, and the mass is proportional to the amplitude of the discontinuity. Here, the inverse problem of optimal focusing reduces to finding the initial profile, when all the particles in the wave period merge simultaneously [17]. In [18], it was shown that simultaneous merging of all particles in the period corresponds to a boundary condition in the form of an inverse saw-tooth wave. A peculiarity of the inverse saw-tooth wave is the formation of a discontinuity of finite amplitude and the universality of the wave profile before and after formation of the discontinuity. In [18], based on these properties, an acoustic turbulence model was constructed as the superpositions of inverse saw-tooth waves of different scale with the Weierstrass–Mandelbrot spatial spectrum.

Let us rewrite the solution for a Riemann wave as follows:

$$\theta(z) = \Phi^{-1}(V) - zV. \qquad (25)$$

On the plane of variables (z, θ), formula (25) gives the family of characteristics of the equation for simple (Riemann) waves:

$$\frac{\partial V}{\partial z} - V\frac{\partial V}{\partial \theta} = 0. \qquad (26)$$

For this equation, the characteristics of (25) are straight lines. The parameter for the family of straight lines is perturbation V. The $\Phi^{-1}(V)$ value determines the point of intersection of characteristic (25) with axis θ for $z = 0$.

The family of characteristics for one period of the initial sinusoidal signal is constructed in Fig. 4. For each of the characteristics, with increasing z, the determined value of perturbation V moves; therefore, it is easy to follow the distortion of the time profile. Curves *1*, *2*, and *3* correspond to distances $z = 0, 0.8, 1.5$. Since the inclination of straight lines (25) to the z axis increases with increasing V, the steep areas of the leading edge in the wave profile are more strongly distorted. Intersection of the characteristics corresponds to discontinuity formation. Clearly, a discontinuity begins to form at a distance of $z = 1$. The size of the jump reaches a maximum for $z = \pi/2$. Comparing Figs. 4 and 3, we see that the shock front formation process, just like nonlinear energy losses, is not concentrated in a narrow region of z values, but "smeared" over a sufficiently extended region. Therefore, a harmonic signal cannot be time-focused well.

The case of "ideal" focusing of the leading half-period of the wave is shown in Fig. 5. The initial profile is composed of segments of straight lines forming the periodic sequence of triangles. Clearly, the character-

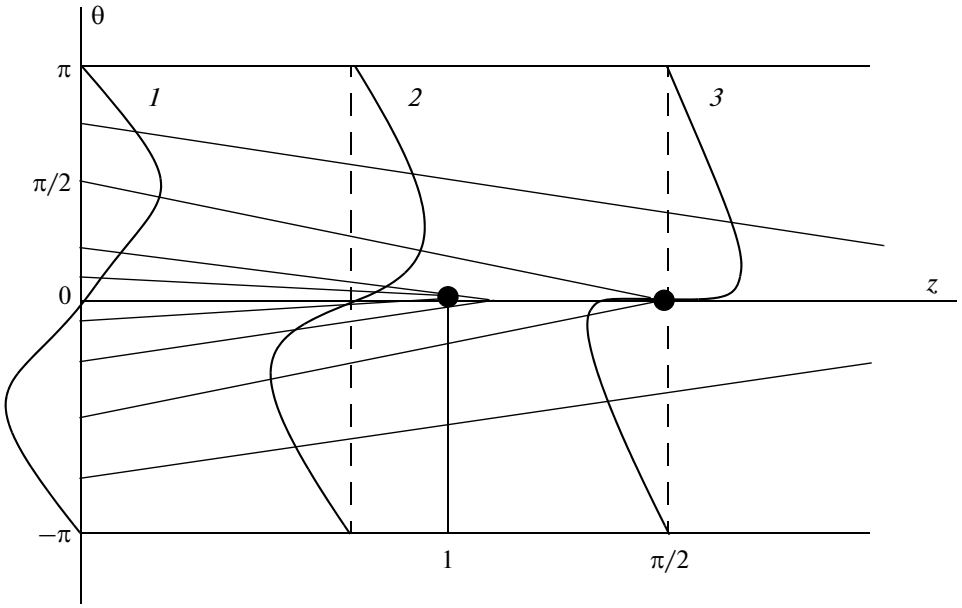

Fig. 4. Family of straight lines—characteristics of Eq. (26) and corresponding constructed profiles of initial time-sinusoidal signal at distance of $z = 0$, 0.8, 1.5 (curves *1*–*3*). Shock front formation begins at $z = 1$, where the characteristics first intersect.

istics coming from the domain $-1 < \theta < 1$, intersect the z axis at one point; i.e., there is no "aberration" of the characteristics. This means that the amplitude of the shock front at point $z = 1$ immediately assumes the maximum value. During subsequent propagation, it begins to decay due to nonlinear attenuation. The thermal and radiation action of the wave on the medium will take place in the domain $z > 1$, with the maximum at point $z = 1$ (cf. Fig. 3).

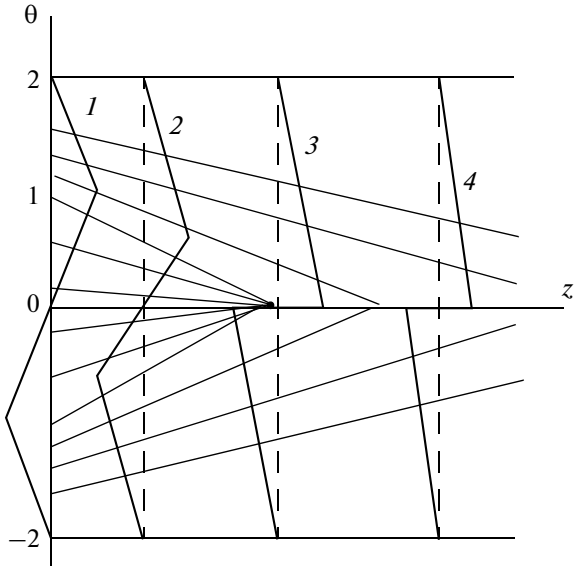

Fig. 5. Family of straight lines—characteristics of Eq. (26) and corresponding constructed profiles of initial saw-tooth (in time) signal at distances of $z = 0$, 0.4, 1.1, 2 (curves *1*–*4*). The shock front forms at point $z = 1$, where some of the family of characteristics corresponding to the leading edge intersect.

We now consider an IPNA for time focusing in the same sense as follows from Figs. 4 and 5, i.e., as the problem of reconstructing the time profile ensuring "aberrationless focusing" of the characteristics. We require that the characteristics intersect at one point $(\theta, z) = (\theta_*, z_*)$ for any values of parameter V. This means that the two relations

$$\theta - \theta_* = \Omega(V)\left(z_* - z\right), \quad \theta - C = \Phi^{-1}(V) - zV \qquad (27)$$

should coincide. However, this is possible only if Φ is a linear function of time θ: $\Phi = \theta/z_*$, i.e., $\Phi^{-1} = z_*V$. Here, $\Omega = V$, $C = \theta_*$. Thus, the characteristics of the leading edge of the wave in Fig. 5 are optimally focused.

INVERSE PROBLEM OF OPTIMAL FOCUSING

As is known, ultrasound action is intensified by increasing its intensity. For this, many industrial and medical applications use focusing devices. However, in a number of problems, the main factor determining the result of the action is not the intensity, but other wave field parameters. Examples are the peak positive pressure of a pulse signal or pressure gradients responsible for ultrasound-induced destruction, e.g., of kidney stones [19] or subcellular structures of cancer cells [20]. The minimum pressure in the wave rarefaction phase determines the development of cavitation in fluids [21]. In addition to the listed parameters, the kinetics of the processes is affected by the duration of

compression and rarefaction zones, the time of shock front growth in the profile of a signal distorted by nonlinearity, and the characteristic frequencies of the harmonics forming this signal. Clearly, for the most effective action on a medium or a target, it is necessary to decide which wave parameters are determining and to synthesize the spatial and temporal structure of the radiated wave that will maximize these parameters in the needed spatial domain.

Ultrasound therapy [22] makes wide use of wave-focusing devices. In the energy concentration process, the role of nonlinear effects significantly increases. In addition to nonlinearity, it is necessary to take into account the complex frequency-dependent dissipative properties of biological tissues, as well as diffraction in the focal region. The role of these factors when calculating the coefficient of field intensification at the focus is discussed in detail in review [23] (sections 5 and 6).

Let us recall that during the propagation of intense acoustic waves, shock fronts form in their profiles, after which wave attenuation sharply intensifies. In modern focusing devices used in medicine, field intensities at the focus reach several kW/cm^2; here, nonlinear wave absorption is larger than linear absorption by an order of magnitude. In many situations, saturation occurs; i.e., far from the source, the wave intensity cannot exceed a certain limit, no matter how much its initial value increases [23].

In nonlinear focusing problems, it is convenient to use the dimensionless form of the KZK equation, which differs from (1):

$$\frac{\partial}{\partial\theta}\left(\frac{\partial V}{\partial z} - NV\frac{\partial V}{\partial\theta} - G\frac{\partial^2 V}{\partial\theta^2}\right) = \frac{D}{4}\left(\frac{\partial^2 V}{\partial R^2} + \frac{1}{R}\frac{\partial V}{\partial R}\right). \quad (28)$$

Here, the following notation is used

$$V = \frac{p}{p_0}, \quad z = \frac{x}{d}, \quad \theta = \omega\tau, \quad R = \frac{r}{a}. \quad (29)$$

In contrast to formula (2), the dimensionless distance is now counted in units of length d (this is the distance from the surface of the source to the geometrical focus point). The dimensionless numbers in Eq. (28) are equal to

$$N = \frac{d}{l_{SH}}, \quad G = \frac{2d}{l_{DISS}}, \quad D = \frac{d}{l_{DIF}}. \quad (30)$$

For these formulas, like before, formulas (3) give the characteristic scales of manifestation of nonlinear, dissipative, and diffraction effects.

Let us present and discuss the solution to Eq. (28) obtained by the successive approximation method for the problem of second harmonic generation. The formulas given below are a simple generalization of the results explained in [24]. The solution of the first approximation has the form

$$V^{(1)} = \frac{1}{f(z)}\exp\left(-Gz - \frac{R^2}{f^2}\right)\sin(\theta + \varphi(z)). \quad (31)$$

Here,

$$f = \sqrt{(1-z)^2 + D^2 z^2},$$
$$\varphi = \arctan\frac{Dz}{1-z} + \pi H(z-1) + \frac{R^2}{f^2}\left(\frac{1-z}{D} - Dz\right), \quad (32)$$

$H(z)$ is the Heaviside function (unit jump).

In the second approximation, we find the expression for the field at the frequency of the second harmonic. In complex representation, it has the form

$$V^{(2)} = -iN\frac{\exp(-4Gz - i2\theta)}{1 - z + iDz}$$
$$\times \exp\left(-2R^2\frac{1 + i/D}{1 - z + iDz}\right)\int_0^z \frac{\exp(2Gy)}{1 - y + iDy}dy. \quad (33)$$

When there is no dissipation in the medium, i.e., $G = 0$, solution (33) is expressed via elementary functions:

$$V^{(2)} = A_2(z, R)\sin(2\theta + \varphi(z, R)). \quad (34)$$

The amplitude and phase of the second harmonic are given by the expressions

$$A_2 = \frac{N}{2\sqrt{1 + D^2}}\frac{1}{f}\exp\left(-\frac{2R^2}{f^2}\right)\left[\varphi_0^2(z) + \ln^2 f\right]^{1/2}, \quad (35)$$

$$\varphi_2 = \varphi_0(z) + \frac{2R^2}{f^2}\left(\frac{1-z}{D} - Dz\right)$$
$$- \arctan\left(\frac{\varphi_0 + D\ln f}{\ln f - D\varphi_0}\right). \quad (36)$$

Here, $\varphi_0 = \varphi(z, R = 0)$ is the phase of the first harmonic on the beam axis.

It is interesting to note that the important physical quantity

$$2\varphi - \varphi_2 = \varphi_0(z) + \operatorname{arctg}\left(\frac{\varphi_0 + D\ln f}{\ln f - D\varphi_0}\right), \quad (37)$$

characterizing the relative phase shift between the waves of the first and second harmonics proves independent of radial coordinate R. This means that if the phase of each of the harmonics strongly changes in the beam cross section, then the resulting profile tangent to the beam will change significantly more slowly.

Figure 6 shows the dependence of phase shift (37) on the distance passed by the wave. The parameter values were assumed equal to $D = 0.5$ (curve *1*) and 0.1 (curve *2*). It is important to consider that the phase shift between the harmonics occurring due to diffraction destroys the shock front and reduces the effectiveness of focused ultrasound action.

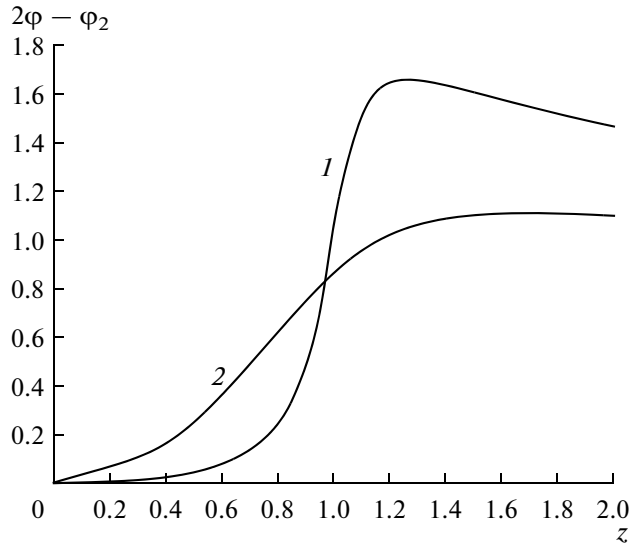

Fig. 6. Distance dependence of phase shift between waves of first and second harmonics. Parameter values taken as follows: $D = 0.5$ (curve *1*) and 0.1 (curve *2*).

In the presence of attenuation, when $G \neq 0$, solution (33) can be expressed via special functions:

$$V^{(2)} = iN\frac{\exp(-4Gz - i2\theta)}{1 - z + iDz} \times \exp\left(-2R^2\frac{1 + i/D}{1 - z + iDz}\right)\frac{1}{1 - iD} \times \exp\left(\frac{2G}{1 - iD}\right)\left[E_1\left(\frac{2G}{1 - iD}\right) - E_1\left(\frac{2G}{1 - iD}(1 - z + iDz)\right)\right]. \quad (38)$$

Here, E_1 is the integral exponential of the complex argument:

$$E_1(\nu) = \int_\nu^\infty \exp(-t)\,dt/t.$$

For small values of the arguments, the expansion $E_1(\nu) \approx -\gamma - \ln\nu + \nu - 0.25\nu^2$, is valid, where γ is the Euler constant. Using this expansion, we obtain a simple expression for the amplitude of the second harmonic on the beam axis:

$$A_2 = \frac{N}{2D}\left[\frac{\pi^2/4 + (\ln D + 2G)^2}{1 + D^2}\right]^{1/2} \times \exp\left(-4G + \frac{2G}{1 + D^2}\right). \quad (39)$$

Formula (39) yields good accuracy for small absorption $G < 0.2$.

In the most interesting case $D \ll 1$, when diffraction is weakly pronounced, the amplitude of the second harmonic at the focus can be calculated by the formula

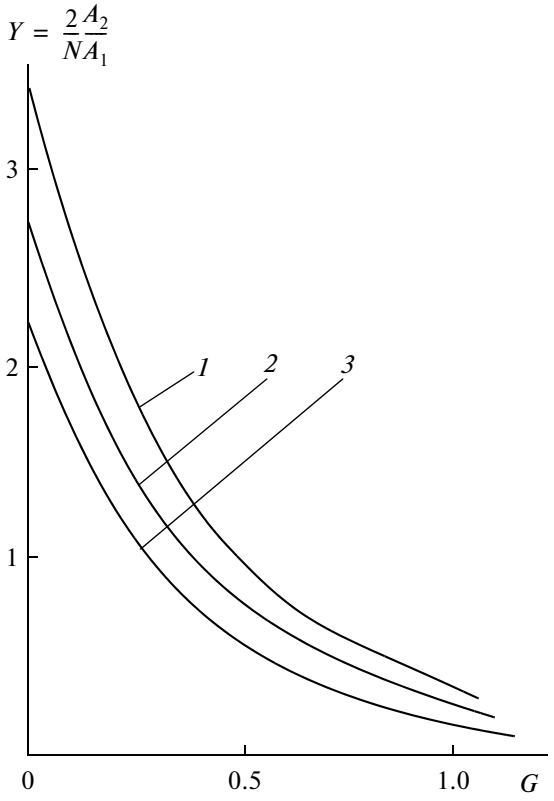

Fig. 7. Dependence of ratio (41) of amplitudes of second and first harmonics at focus on number G (30). Values of parameter D: 0.05 (curve *1*), 0.1 (curve *2*), and 0.2 (curve *3*).

$$A_2 = \frac{N}{2D}\exp(-2G) \times \left\{\left[E_1(2G) + \mathrm{Ci}(2GD)\right]^2 + \left[\frac{\pi}{2} - \mathrm{Si}(2GD)\right]^2\right\}^{1/2}. \quad (40)$$

Here, Si, Ci are the integral sine and cosine. Using formula (40) and special function tables, we can calculate the ratio of the amplitudes of the second and first harmonics at the focus:

$$Y = \frac{2}{N}\frac{A_2}{A_1}. \quad (41)$$

The corresponding curves are shown in Fig. 7. Based on these data, we can easily estimate the limits of applicability of the successive approximation method. We use the criterion $A_2/A_1 \leq 0.1$. For example, for values of $G = 1$, $D = 0.1$ we find the limiting value $N \approx 0.87$, for which calculation by the successive approximation method yields reliable results.

This method has a drawback: it can only calculate weak lower harmonics. The paraxial approach is more fruitful, making it possible to describe near the beam axis strongly distorted wave profiles containing a large number of harmonic spectral components. The solu-

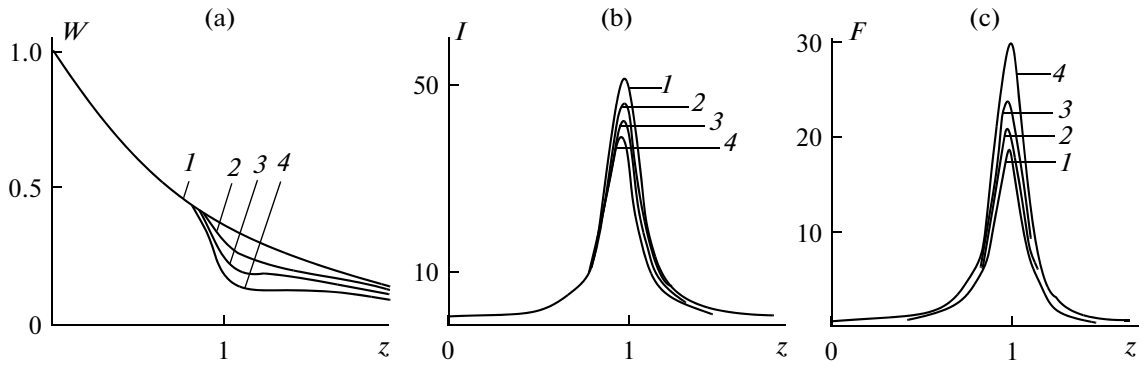

Fig. 8. Distance dependence of power (a), intensity (b), and radiation force (c). Parameter values: $D = 0.1$, $G = 0.5$.

tion to KZK equation (28) using the paraxial approach is sought in the form of an expansion into a series of coordinates orthogonal to the beam axis [25]. Here, we will use the results of the latest modified version [26, 27] of the paraxial approximation. For the wave intensity, in particular, the following formula is obtained:

$$I = \overline{V^2} = \frac{1 - Q^2(\eta)}{2f^2(\eta)} \exp\left(-\frac{2R^2}{f^2(1 - Q^2)}\right). \quad (42)$$

Here, an auxiliary spatial coordinate η was used, related to the normalized distance z along the beam axis by

$$\eta(z) = \varphi = \arctan\frac{Dz}{1 - z} + \pi H(z - 1). \quad (43)$$

Note that η formally coincides with expression (32) for the phase of the first harmonic on the beam axis. Other notation in formula (42) is as follows:

$$f(\eta) = \frac{D}{\sin\eta + D\cos\eta},$$
$$Q(\eta) = \frac{N}{\sqrt{2}}\frac{D}{1 + D^2}\left(\frac{\ln f}{f} + \eta\frac{d}{d\eta}\frac{1}{f}\right). \quad (44)$$

Numbers N, D introduced earlier (30) increase with the corresponding increasing nonlinearity or diffraction.

Integrating intensity (42) over the beam cross section, we find the total power:

$$W = \frac{\pi}{4}\left(1 - Q^2(\eta)\right)^2. \quad (45)$$

Formulas (42) and (45) can be modified by introducing absorption. Here, the power will be equal to

$$W = \frac{\pi}{4}\exp(-2Gz)\left[1 - \exp(-2Gz)Q^2(\eta)\right]^2, \quad (46)$$

and the intensity on the beam axis

$$I = \frac{\exp(-2Gz)}{2f^2(\eta)}\left[1 - \exp(-2Gz)Q^2(\eta)\right]. \quad (47)$$

Let us now analyze the radiation force. Averaging with the solutions presented in [26] and modifying them for the case of an absorbing medium [27], we obtain

$$F = \overline{\left(\frac{\partial V}{\partial\theta}\right)^2} = \frac{1}{2f^2\sqrt{1 - \gamma^2}}\exp\left(-\frac{2R^2}{f^2} - 2Gz\right)$$
$$\times\left[1 + \cos(2\eta - 2\beta)\frac{1}{\gamma^2}\left(\sqrt{1 - \gamma^2} - 1\right)^2\right]. \quad (48)$$

Here we denote

$$\gamma = \frac{N}{\sqrt{1 + D^2}}\exp(-Gz)\sqrt{\eta^2 + \ln^2 f},$$
$$\beta = \arctan\left(\frac{\eta + D\ln f}{D\eta - \ln f}\right). \quad (49)$$

The domain of applicability of formula (48) is limited by the condition $\gamma < 1$. Since the validity of this solution for the radiation force can be violated near the focus, we set $z = 1$ (or $\eta = \pi/2$) in formula (49) for γ, after which the condition $\gamma < 1$ reduces to the following restriction:

$$N < \left(\frac{1 + D^2}{\pi^2/4 + \ln^2 D}\right)^{1/2}\exp(G). \quad (50)$$

In particular, in the most interesting case of weak diffraction and mild attenuation, the nonlinearity can be quite strongly pronounced. For example, for values of $D = 0.1$ and $G = 1$, from formulas (50) we obtain $N < 1.25$.

The behavior of power (46), intensity (47), and radiation force (48) for an increase in axial coordinate z is shown in Fig. 8 The parameter values are assumed equal to $D = 0.1$, $G = 0.5$. Manifestations of nonlinearity are intensified with increasing curve number: $N = 0.01$ (curve *1*), 0.3 (*2*), 0.4 (*3*), and 0.5 (*4*). Similar curves are shown in Fig. 9 for different parameter values: $D = 0.5$, $G = 0.5$, $N = 0.01$, 0.4, 0.7, and 1 (curves *1–4*, respectively).

In Fig. 8a one can see that the gradual decrease in power caused by dissipation occurs only at the initial focusing stage. Near the geometric focus $z = 1$, a dip occurs, related to the "switching on" of nonlinear

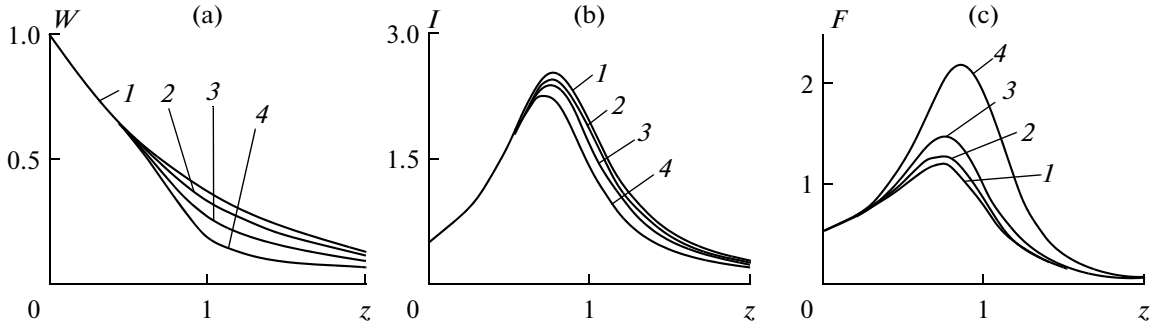

Fig. 9. Distance dependence of power (a), intensity (b), and radiation force (c). Parameter values $D = 0.5$, $G = 0.5$.

absorption owing to the sharp increase in the wave amplitude during its convergence. This dip worsens with increasing nonlinearity—with increasing number N.

Figure 9a was constructed for a large value of diffraction parameter D. Here, the amplification of the field at the focus is not as significant. Therefore, the dip on the curve for the power turns out to be not as sharp or deep.

The intensification of the field in the focal region can be judged from Figs. 8b and 9b, constructed for the mean wave intensity on the beam axis.

Figures 8c and 9c show the behavior of the radiation force with an increase in distance z. An increase in nonlinearity leads to an increase in the peak value of the force and a decrease in the area of its spatial localization.

Figure 10 shows how the data of Figs. 8 and 9 can be used for the specific problem of radiation action on liver tissue [2], e.g., for measuring its shear elasticity by the SWEI method [28]. The curves show the change

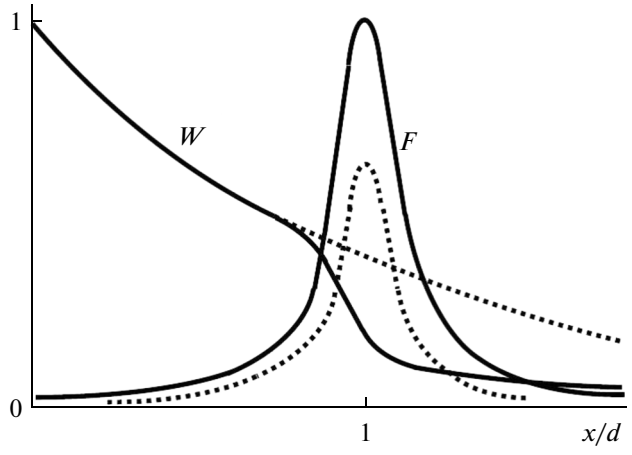

Fig. 10. Change with distance of power W in focused beam and radiation force F. Dashed curves correspond to linear dissipative medium; solid curves are constructed taking into account nonlinearity (ratio of focal distance d to length of discontinuity formation l_{SH} is 0.5).

along the axis of the total power W in the beam focused on an absorbing biological tissue (liver) and the radiation force F. The temperature increment appearing as a result of ultrasound absorption qualitatively behaves the same as F. The influence of nonlinearity (solid curves) is characterized by the ratio of focal distance d to the length of discontinuity formation l_{SH}, 0.5. Clearly, the power first gradually decreases with distance due to linear dissipative losses; near the focus, a dip appears, caused by nonlinear attenuation. The intensity at the focus reaches a maximum; its value decreases due to nonlinear losses at the shock front. In contrast, the values of the peaks of the radiation force and temperature increase with an increase in nonlinearity, and their widths characterizing the locality of the action, decrease.

If shock fronts form in the region between the transducer and the focus, nonlinear losses lead to a decrease in the linear (for weak waves) value of the focuser amplification coefficient K. However, in the presence of diffraction, nonlinearity may not only decrease, but also increase K due to the "sharper" focusing of higher harmonics generated by the wave of the main frequency [29]. This occurs when nonlinear attenuation going to the focus does not lead to appreciable energy losses, i.e., a saw-tooth wave, if one forms, directly before the focus. Hence it follows that, to obtain large K values, the nonlinear focusing parameters should be optimized by solving the IPNA.

In many applications, a high locality of ultrasound is required. For this, it is necessary to create the largest radiation forces, temperature increments, or steep shock fronts in a small volume of a medium. Meanwhile, diffraction phase shifts between the harmonics can increase the width of the shock front, thereby decreasing the maximum of the radiation force (temperature) and increasing the dimensions of its localization area. This undesirable effect can be compensated by synthesizing on the transducer a profile of complex form with certain relations of the amplitudes and phases between the components of its frequency spectrum. These relations are chosen such that the joint effect of nonlinearity, diffraction, and dissipation

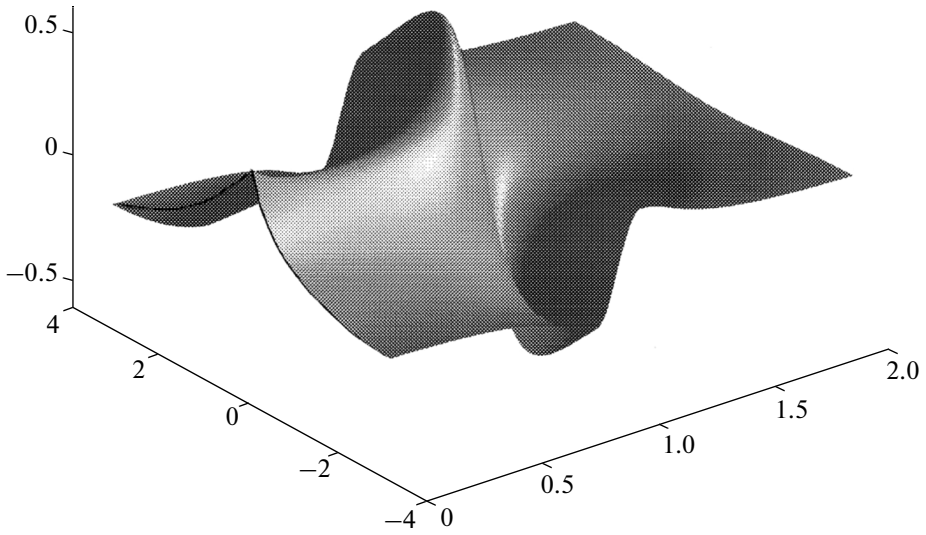

Fig. 11. Example of solution to nonlinear inverse problem of synthesizing profile of wideband periodic wave, which as a result of joint action of nonlinearity, diffraction, and dissipation near focus transforms to a discontinuous saw-tooth wave.

leads to the formation of a shock front directly at the focus. Thus, it is possible to transport high energy densities (without substantial losses on the way from the transducer to the focus) and organize local energy discharge in the focal region, having "switched on" here nonlinear absorption.

To synthesize the special shape of the profile, it is necessary to solve the nonlinear inverse problem [1, 2]. Figure 11 shows the corresponding example. Clearly, the anharmonic smooth profile (one period is shown) is transformed during propagation, becoming discontinuous as it approaches the focus.

Modern focusing systems ensure rapid heating of tissue in the focal region by tens of degrees within times on the order of seconds, so that natural cooling by intensified blood flow (perfusion) cannot occur. At high temperatures denaturation of protein molecules, embolism of blood vessels, and destruction of tissues, including tumorous neoplasms, occur. A change in the structure of irradiated tissues and an increase in "hardness" lead to intensification of their scattering properties and an increase in shear elasticity. In principle, temperature can also be measured remotely in undamaged tissues by acoustic thermography [30] (by thermal acoustic radiation at frequencies on the order of megahertz) and insonification of the heated region [31].

CONCLUSIONS

Nonlinear inverse problems, especially those related to the use of strongly distorted nonlinear waves, is a new important direction, which, in the authors' opinion, should attract the attention of not only acousticians, but also mathematicians and specialists in the field of nonlinear wave theory and medical ultrasound. The aim of this review is to interest readers in continuing this research.

ACKNOWLEDGMENTS

This work is supported by the Russian Science Foundation. Studies performed at Nizhny Novgorod University are supported by grant no. 14-12-00882, and at Moscow University, by the grant no. 14-12-00042.

REFERENCES

1. O. V. Rudenko, High-power focused ultrasound: Nonlinear phenomena, shear wave excitation and medical diagnostics, in Khokhlov Readings (Moscow State Univ., 1996) [in Russian].
2. O. V. Rudenko, Moscow Univ. Phys. Bull., 51, 18 (1996).
3. V. A. Burov, I. E. Gurinovich, O. V. Rudenko, and R. Ya. Tagunov, Acoust. Phys., 40, 816 (1994).
4. V. A. Burov, A. A. Shmelev, and D. I. Zotov, Acoust. Phys. 59, 31 (2013).
5. O. V. Rudenko and Chin An Wu, Acoust. Phys. 40, 668 (1994).
6. Yu. R. Lapidus and O. V. Rudenko, Sov. Phys. Acoust. 36, 589 (1990).
7. O. V. Rudenko and S. I. Soluyan, Dokl. Akad. Nauk 298, 361 (1988).
8. O. V. Rudenko, Rus. J. Nondestructive Testing, 29, 583 (1993).
9. O. V. Rudenko, Phys.-Usp., 49, 69 (2006).
10. O. V. Rudenko, Phys.-Usp., 50, 359 (2007).
11. O. V. Rudenko, in Nonlinear Waves (Inst. Appl. Phys. Russ. Acad. Sci., 2012), pp. 189–204 [in Russian].
12. O. V. Rudenko, Acoust. Phys., 56, 457 (2010).

13. M. B. Vinogradova, O. V. Rudenko, and A. P. Sukhorukov, Theory of Waves, (Lenand, Moscow, 2015), 3rd ed., [in Russian].
14. O. V. Rudenko, S. N. Gurbatov, and C. M. Hedberg, Nonlinear Acoustics through Problems and Examples, (Trafford, Canada, 2010).
15. S. N. Gurbatov, O. V. Rudenko, and A. I. Saichev, Waves and Structures in Nonlinear Nondispersive Media, (Fizmatlit, Moscow, 2008) [in Russian].
16. S. N. Gurbatov, O. V. Rudenko, and A. I. Saichev, Waves and Structures in Nonlinear Nondispersive Media: General Theory and Applications to Nonlinear Acoustics, (Springer-Verlag, Berlin 2011).
17. S. N. Gurbatov and O. V. Rudenko, Radiophys. Quant. Electron., 58, 463 (2015).
18. S. N. Gurbatov and A. V. Troussov, J. Phys. D: Appl. Phys. 145, 47 (2000).
19. V. G. Andreev, V. Yu. Veroman, G. A. Denisov, O. V. Rudenko, and O. A. Sapozhnikov, Sov. Phys. Acoust. 38, 325 (1992).
20. V. A. Burov, N. P. Dmitrieva, and O. V. Rudenko, Dokl. Biochemistry and Boiphysics, 383, 101 (2002).
21. V. A. Akulichev, in High-Intensity Ultrasonic Fields, Ed. by L. D. Rozenberg, (Plenum, New York, 1971).
22. O. V. Rudenko, Herald Russ. Acad. Sci. 78, 7 (2008).
23. O. V. Rudenko, Phys.-Usp., 38, 965 (1995).
24. O. V. Rudenko, and S. I. Soluyan, Theoretical Foundations of Nonlinear Acoustics, (Plenum, New York, 1977).
25. O. V. Rudenko, S. I. Soluyan, and R. V. Khokhlov, Sov. Phys. Dokl., 20, 836 (1975).
26. M. F. Hamilton, V. A. Khokhlova, and O. V. Rudenko, J. Acoust. Soc. Am., 101, 1298 (1997).
27. O. V. Rudenko, A. P. Sarvazyan, and S. Y. Emelianov, J. Acoust. Soc. Am., 99, 2791 (1996).
28. A. P. Sarvazyan, O. V. Rudenko, S. D. Swanson, J. B. Folwkes, and S. Y. Emelianov, Ultrasound Medic. Biol., 24, 1419 (1998).
29. K. Naugolnykh and L. A. Ostrovskii, Nonlinear Wave Processes in Acoustics (Cambridge Univ., Cambridge, 1998).
30. V. A. Burov, P. I. Darialashvili, S. N. Evtukhov, and O. D. Rumyantseva, Acoust. Phys., 50, 243 (2004).
31. V. G. Andreev, A. V. Vedernikov, A. V. Morozov, and V. A. Khokhlova, Acoust. Phys., 52, 119 (2006).

Translated by A. Carpenter